Attitude Stabilization Using Two Parallel Single-Gimbal Control Moment Gyroscopes

Chengfei Yue*
National University of Singapore, Singapore 119077, Republic of Singapore
Krishna Dev Kumar†
Ryerson University, Toronto, Ontario M5B 2K3, Canada
and
Qiang Shen,‡ Cher Hiang Goh,§ and Tong Heng Lee¶
National University of Singapore, Singapore 119077, Republic of Singapore

DOI: 10.2514/1.G003445

This paper investigates the underactuated attitude stabilization problem using two parallel single-gimbal control moment gyroscopes (SGCMGs). Different from most existing underactuated control techniques requiring the zero total angular momentum assumption, only the controllability of the whole control moment gyroscope (CMG)–spacecraft system, which means the total angular momentum of the spacecraft with CMG array within the momentum envelope of the CMG array, is required in this paper. To achieve the underactuated attitude stabilization, a new controller consisting of two parts, that is, a higher level sliding mode control part to stabilize the angular velocity about the underactuated axis in finite time and a tracking control part to track desired angular velocities that are used to stabilize the remaining states, is developed. This proposed novel control logic achieves attitude stabilization when the initial total angular momentum of the CMG-spacecraft is not zero. Simulations show that the attitude of a microsatellite can be stabilized precisely within acceptable time using the proposed control law and steering law when the controllability constraint is satisfied. When the initial total momentum of the spacecraft base and the CMG array exceeds the momentum envelope of the CMG array, simulation results demonstrate that the attitude is controlled to be a periodic oscillation in the vicinity of the equilibrium, at the same angular momentum level determined by the initial condition.

I. Introduction

SPACECRAFT attitude control is a fundamental problem in spacecraft application, but the results on underactuated cases are not as common. Most of existing results are obtained when the spacecraft is fully actuated. Although this is true for most of the spacecraft, failures occur occasionally. Almost 30% of all failures are caused by actuators, and out of them two-thirds are caused by control moment gyroscopes (CMGs), reaction wheels (RWs), and momentum wheels (MWs) [1]. When the remaining actuators cannot provide three-axis control torque, the spacecraft attitude control system degrades to an underactuated system. There is a growing interest in developing attitude control strategies for underactuated systems to maintain partial or complete control performance, enhance reliability of attitude control system, simplify collocation of actuators, decrease cost, economize energy, and so on.

For the underactuated system, the actuator is another key issue for the control system design. Thrusters provide control torque by consuming propellant. This kind of control torque is external torque and the spacecraft dynamic equation is not influenced by the integration of thrusters. Compared with thrusters, momentum exchange devices have significant advantages of cleanliness, without the expulsion of gases that may blur the payloads and sensors, and precision. However, employing momentum exchange devices as actuators increases the complexity of controller design because the angular momentum and the dynamics of the actuators should be considered simultaneously in the controller design. Among the momentum exchange devices, RW and single-gimbal control moment gyroscope (SGCMG)–actuated control systems have been widely studied [2–5]. For RWs, the generated output control torque lies in the same direction as the input control command. For the CMGs, there exists a high nonlinearity from input to output, and the trigonometric functions are governed by the gimbal angles. Besides, the Jacobian matrix may lose rank and consequently singularity occurs. In such cases, there is no output in some specific direction and the three-axis controllability is lost at these time instants [6,7]. To avoid/escape singularity and map the control torque to the gimbal angular velocity domain precisely, one approach is to consider the gimbal dynamics simultaneously in the controller design process and compute the gimbal speed directly as in [8], and other approach is to develop different steering laws as in [9–11]. Most of these proposed steering laws are designed for redundant CMG cluster. Even though they can be extended to the underactuated system, the performance may be degraded. Thus investigating the underactuated CMG-spacecraft system and developing a suitable steering law is of considerable importance.

To achieve three-axis attitude stabilization of underactuated CMG-spacecraft system, the controllability of such systems should be addressed. Using geometric control theory, Crouch gave necessary and sufficient conditions in the cases of one, two, or three independent torques. It is stated that a spacecraft using fewer than three momentum exchange devices is uncontrollable on the six-dimensional state-space defined by a three-parameter attitude representation and angular velocity [12]. Bhat and Tiwari further investigated the CMG-actuated spacecraft system and proved the controllability of the spacecraft containing one or more CMGs in the invariant manifold, that is, invariant hypersurface in the state space determined by the angular momentum conservation property. They derived a sufficient condition for controllability of two-SGCMG

Received 9 November 2017; revision received 16 January 2019; accepted for publication 21 January 2019; published online 15 March 2019.

*Ph.D. Student, Department of Electrical and Computer Engineering, 4 Engineering Drive 3, Singapore 117583, Republic of Singapore; also Visiting Ph.D. Student, Department of Aerospace Engineering, 350 Victoria Street (Corresponding Author).

†Professor, Department of Aerospace Engineering, 350 Victoria Street.

‡Also Research Scientist, Temasek Laboratories, 4 Engineering Drive 3, Singapore 117583, Republic of Singapore.

§Also Adjunct Professor, Department of Electrical and Computer Engineering, 4 Engineering Drive 3, Singapore 117583, Republic of Singapore.

¶Also Professor, Department of Electrical and Computer Engineering, 4 Engineering Drive 3, Singapore 117583, Republic of Singapore.

spacecraft. It states that the spacecraft is controllable if the initial momentum of the whole system is within the CMGs' angular momentum envelope [13]. This motivates the study of spacecraft attitude control with one [14] or two CMGs [15,16].

For the attitude control strategy, Tsiotras and Doumtchenko investigated the control of spacecraft subject to actuator failures [17]. The control problem was divided into angular velocity stabilization and complete attitude stabilization. Yamada et al. worked on the rate damping of spacecraft with two arbitrarily configured SGCMGs [18]. Rate damping is achieved when the angular momentum of CMG-spacecraft system is less than the sum of the angular momentum of the CMG array; otherwise, the spacecraft settles to a spinning motion. Different from the rate damping problem, complete global attitude stabilization with arbitrary initial conditions conflicting with Bhat's controllability condition is not possible [13]. However, partial attitude stabilization under some restricted assumption or in some constrained manifold is still possible. Gui et al. investigated the attitude stabilization of a rigid spacecraft with two parallel CMGs [19] or two skew CMGs [20]. In these works, the initial angular momentum of the CMG-spacecraft system is assumed to be zero. Under this assumption, the dynamic system can be simplified as a two-axis system and attitude stabilization is achieved. However, this assumption is conservative for the CMG actuated system compared with the controllability condition stated in [13]. Thus developing a controller to achieve complete attitude stabilization when the controllability is satisfied and remove the unnecessary restrictions is important.

Motivated by the aforementioned observation, this paper develops a controller to stabilize the underactuated CMG-spacecraft without the zero total angular momentum requirement of the CMG-spacecraft system. First, we set the desired angular velocity about the axis without control input, that is, ω_{dz}, to be zero. Then the desired lateral rates, that is, ω_{dx} and ω_{dy}, are designed to stabilize the complete kinematics. To track this desired angular velocities about the axes with control input, a feedback control part with feedforward compensation is developed. Second, by employing the sliding mode control technique, the dynamic coupling effect is exploited to track the desired angular velocity, which is set to zero. This is equivalent to stabilizing the angular velocity ω_z about the underactuated axis. Therefore, complete attitude stabilization without the zero total angular momentum requirement is achieved under the joint control of the rate command tracking about the actuated axes and the angular velocity damping about the underactuated axis simultaneously. To realize the control torque demanded by the controller, a new steering law with low-computation is developed. To compute the inverse of the specific 2-by-2 Jacobian matrix ($\boldsymbol{A}^{-1}$), the determinant ($\det(\boldsymbol{A})$) and adjoint matrix ($\boldsymbol{A}^*$) are calculated to get $\boldsymbol{A}^{-1} = \boldsymbol{A}^*/\det(\boldsymbol{A})$ when $\det(\boldsymbol{A}) \neq 0$. When CMG singularity occurs, the Jacobian matrix is rank deficient and not invertible ($\det(\boldsymbol{A}) = 0$). To escape the singularity region, we modify the calculated determinant of the Jacobian matrix by adding a small offset δ_e such that $\det(\boldsymbol{A}) \neq 0$. This determinant modification, a small increment of the denominator in calculating matrix inverse, introduces a smaller torque error compared with the global singular robust steering law using the time-varying perturbation.

The rest of the paper is organized as follows. Section II presents the system mathematical model, the CMG model, dynamics and kinematics, and controllability determined by the initial angular momentum. Section III addresses the controller design procedure step by step. Section IV presents the proposed steering law. A comparison study with the global singular robust steering law is presented. Using the proposed controller and steering logic, simulation results are shown in Sec. V. Finally, conclusions are noted in Sec. VI.

II. System Model

A. Parallel CMGs

Consider the case that two identical parallel SGCMGs are adopted as actuators, as shown in Fig. 1. Each of the CMG contains a constant-speed rotor. The direction of the rotors' angular momentum is denoted as a unit vector $\boldsymbol{h}_i$. The gimbal rotates about the gimbal axis $\boldsymbol{g}_i$ orthogonal to $\boldsymbol{h}_i$ with a gimbal angular velocity $\dot{\delta}_i$. The gyro output $\boldsymbol{\tau}_i$ in the direction of $\boldsymbol{g}_i \times \boldsymbol{h}_i$ is perpendicular to both $\boldsymbol{g}_i$ and $\boldsymbol{h}_i$. These unit vectors form an orthogonal CMG body coordinate frame denoted as $\mathbb{G}_i = \{\boldsymbol{g}_i, \boldsymbol{h}_i, \boldsymbol{\tau}_i\}$, with the subscript i denoting the ith CMG. As shown in Fig. 2, both the gimbal axes of these two CMGs are along the Z axis in the body frame $\mathcal{F}_B = \{X_B, Y_B, Z_B\}$. Then the angular momentum of the CMGs expressed in $\mathcal{F}_B$ is determined by the magnitude of the rotor's angular momentum h_0 and the gimbal angle $\boldsymbol{\delta} = [\delta_1, \delta_2]^T$, when both $\boldsymbol{h}_1$ and $\boldsymbol{h}_2$ are initially about the X axis and the positive δ_i is generated by a rotation about Z axis:

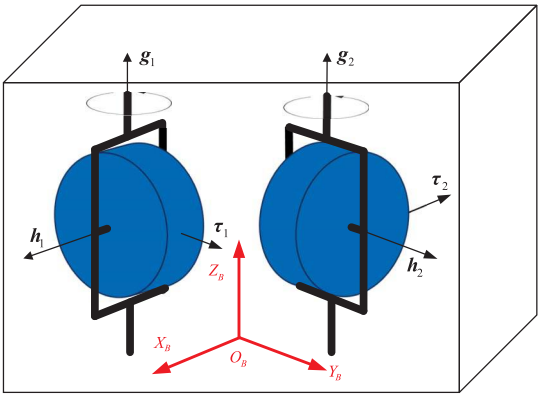

Fig. 1 Spacecraft with two parallel CMGs when $\delta_1 = 0$ and $\delta_2 = (\pi/2)$.

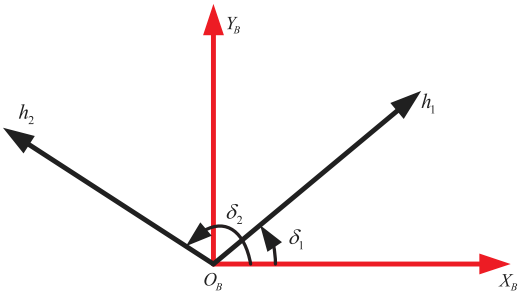

Fig. 2 Angular momentum in the body-fixed frame $\mathcal{F}_B$.

$$\boldsymbol{h}_c = \begin{bmatrix} h_x \\ h_y \end{bmatrix} = h_0 \begin{bmatrix} \cos\delta_1 + \cos\delta_2 \\ \sin\delta_1 + \sin\delta_2 \end{bmatrix} \tag{1}$$

where the subscript "c" represents CMG.

It can be seen that the angular momentum of this parallel CMG array is limited in the X–Y plane and there is no angular momentum along the Z axis parallel to the gimbal axes.

For a momentum exchange device, the output torque $\boldsymbol{\tau}_c$ equals to $-\dot{\boldsymbol{h}}_c$ and can be expressed as:

$$\boldsymbol{\tau}_c = \begin{bmatrix} \tau_{cx} \\ \tau_{cy} \end{bmatrix} = -h_0 \begin{bmatrix} -\sin\delta_1 & -\sin\delta_2 \\ \cos\delta_1 & \cos\delta_2 \end{bmatrix} \begin{bmatrix} \dot{\delta}_1 \\ \dot{\delta}_2 \end{bmatrix} = -h_0 \boldsymbol{A}\dot{\boldsymbol{\delta}} \tag{2}$$

with matrix $\boldsymbol{A}$ being the Jacobian matrix.

B. Spacecraft Dynamics

The total angular momentum of the spacecraft and CMG array, $\boldsymbol{H}_t$, can be expressed as:

$$\boldsymbol{H}_t = \boldsymbol{J}\boldsymbol{\omega} + \boldsymbol{h} \tag{3}$$

where $\boldsymbol{J} = \mathrm{diag}([J_x, J_y, J_z]) \in \mathbb{R}^{3\times3}$ is the moment of inertia of the whole CMG-spacecraft system. The angular momentum arising from the gimbal motion is assumed to be small, implying that the gimbal moments of inertia are negligible, and therefore it is neglected in Eq. (3) [19,21]. $\boldsymbol{\omega} \in \mathbb{R}^3$ is the angular velocity of the spacecraft bus with respect to an inertial frame $\mathcal{F}_I = \{X_I, Y_I, Z_I\}$, and expressed in the body-fixed frame $\mathcal{F}_B$. $\boldsymbol{h} = [\boldsymbol{h}_c^T, 0]^T$, with $\boldsymbol{h}_c$ defined by Eq. (1).

Applying Euler's theorem to Eq. (3), we obtain the attitude dynamics equation as:

$$\boldsymbol{J}\dot{\omega} = -\boldsymbol{\omega}^{\times}(\boldsymbol{J}\boldsymbol{\omega} + \boldsymbol{h}) - \dot{\boldsymbol{h}} \tag{4}$$

where $(\cdot)^{\times}$ denotes a skew-symmetric matrix corresponding to the operation $\boldsymbol{a}^{\times}\boldsymbol{b} = \boldsymbol{a} \times \boldsymbol{b}$, and $\dot{\boldsymbol{h}}$ is the time derivative of $\boldsymbol{h}$ in the body frame. In this paper, similar to [21,22], the external disturbances and gimbal friction are not considered.

Expanding Eq. (4) with $\tau_i = -\dot{h}_i$, $(i = x, y, z)$ and $\tau_z = h_z = 0$, we obtain:

$$\begin{cases} J_x\dot{\omega}_x = (J_y - J_z)\omega_y\omega_z + \omega_z h_y + \tau_x \\ J_y\dot{\omega}_y = (J_z - J_x)\omega_x\omega_z - \omega_z h_x + \tau_y \\ J_z\dot{\omega}_z = (J_x - J_y)\omega_x\omega_y + \omega_y h_x - h_y\omega_x \end{cases} \tag{5}$$

where τ_x and τ_y are the torques produced by the CMGs. This equation demonstrates that ω_z can be controlled through the nonlinear coupling with the transverse rate ω_x, ω_y and the CMG momentum h_x and h_y even when there is no actuator to produce a Z torque.

C. Kinematics

Spacecraft attitude can be expressed by the attitude direction cosine matrix $\boldsymbol{R}$, which describes the spacecraft orientation of body frame $\mathcal{F}_B$ relative to the inertial frame $\mathcal{F}_I$. However, there are nine parameters, not all of which are independent, in the rotation matrix $\boldsymbol{R}$. Instead of the coordinate transformation matrix, a nonsingular parameter of unit quaternion is chosen to describe the spacecraft attitude as $\boldsymbol{Q} = [\,q_0 \quad \boldsymbol{q}_v^T\,]^T$, with q_0 being the scalar part of the $\boldsymbol{Q}$ and $\boldsymbol{q}_v = [q_1, q_2, q_3]^T$ being the vector part. Let $\boldsymbol{Q}$ be the orientation of the spacecraft body frame $\mathcal{F}_B$ with respect to the inertial frame $\mathcal{F}_I$. Then the kinematics of the spacecraft is governed by:

$$\dot{\boldsymbol{Q}} = \begin{bmatrix} \dot{q}_0 \\ \dot{\boldsymbol{q}}_v \end{bmatrix} = \frac{1}{2}\begin{bmatrix} -\boldsymbol{q}_v^T \\ q_0\boldsymbol{I}_3 + \boldsymbol{q}_v^{\times} \end{bmatrix}\boldsymbol{\omega} \tag{6}$$

Then the relationship of $\boldsymbol{R}$ and $\boldsymbol{Q}$ is:

$$\boldsymbol{R}(\boldsymbol{Q}) = \left(q_0^2 - \boldsymbol{q}_v^T\boldsymbol{q}_v\right)\boldsymbol{I}_3 + 2\boldsymbol{q}_v\boldsymbol{q}_v^T - 2q_0\boldsymbol{q}_v^{\times} \tag{7}$$

and a vector $\boldsymbol{Y}_B$ expressed in $\mathcal{F}_B$ can be transformed to the vector $\boldsymbol{Y}_I$ expressed in $\mathcal{F}_I$ by:

$$\boldsymbol{Y}_I = \boldsymbol{R}(\boldsymbol{Q})^T\boldsymbol{Y}_B \tag{8}$$

D. System Controllability

Considering the two-CMG–actuated system without any external torque, the total angular momentum will be conserved in the inertial frame $\mathcal{F}_I$. Thus all the angular momentum states lie in the invariant hypersurface in the state space determined by the initial angular momentum of the whole spacecraft-CMG system. For the initial angular momentum $\boldsymbol{H}_t(t_0)$ and the final value $\boldsymbol{H}_t(t_f)$ expressed as in Eq. (3) with the corresponding attitude $\boldsymbol{Q}_0$ and $\boldsymbol{Q}_f$, they should be equal when they are expressed in $\mathcal{F}_I$:

$$\boldsymbol{R}(\boldsymbol{Q}_0)^T\boldsymbol{H}_t(t_0) = \boldsymbol{R}(\boldsymbol{Q}_f)^T\boldsymbol{H}_t(t_f) \tag{9}$$

For the attitude stabilization problem, the desired attitude $\boldsymbol{Q}_f$ is set to be $\boldsymbol{Q}_f = [1, 0, 0, 0]^T$ when the body-fixed frame $\mathcal{F}_B$ coincides with the inertial frame $\mathcal{F}_I$. Then $\boldsymbol{R}(\boldsymbol{Q}_f)$ becomes $\boldsymbol{I}_3$. Equation (9) can be further expanded by substituting Eq. (3):

$$\boldsymbol{R}(\boldsymbol{Q}_0)^T\left(\boldsymbol{J}\boldsymbol{\omega}(t_0) + \boldsymbol{h}(t_0)\right) = \boldsymbol{J}\boldsymbol{\omega}(t_f) + \boldsymbol{h}(t_f) \tag{10}$$

where $\boldsymbol{\omega}(t_0)$ and $\boldsymbol{\omega}(t_f)$ are the initial and final angular velocities of the spacecraft at the time instants $t = t_0$ and $t = t_f$; $\boldsymbol{h}(t_0)$ and $\boldsymbol{h}(t_f)$ are the initial and the final states of angular momentum of the CMG-array.

Then $\boldsymbol{\omega}(t_f)$ can be calculated from Eq. (10) as:

$$\boldsymbol{\omega}(t_f) = \boldsymbol{J}^{-1}\left\{\left[\boldsymbol{R}(\boldsymbol{Q}_0)^T\left(\boldsymbol{J}\boldsymbol{\omega}(t_0) + \boldsymbol{h}(t_0)\right)\right] - \boldsymbol{h}(t_f)\right\} \tag{11}$$

It should be noted that the angular velocity $\boldsymbol{\omega}$ is always expressed in the body frame. When the attitude stabilization is completed at $t = t_f$, the body frame coincides with the inertial frame, and the expressions of $\boldsymbol{\omega}$ in body frame and in the inertia frame are the same.

Bhat's controllability theory implies that we can always find a final state of CMGs $\boldsymbol{h}(t_f) = [\boldsymbol{R}(\boldsymbol{Q}_0)^T(\boldsymbol{J}\boldsymbol{\omega}(t_0) + \boldsymbol{h}(t_0))]$ when the total angular momentum of the spacecraft system ($\boldsymbol{H}_t(t_0) = \boldsymbol{J}\boldsymbol{\omega}(t_0) + \boldsymbol{h}(t_0)$) lies within the momentum envelope of the CMG array. In such cases, $\boldsymbol{\omega}(t_f) = 0$, which implies that the dynamic system can be completely stabilized and the rotations will cease. Then we can find a proper controller to render the initial attitude $\boldsymbol{Q}_0$ to the desired $\boldsymbol{Q}_f$. Otherwise, $\boldsymbol{\omega}(t_f) \neq 0$ and complete attitude stabilization is not possible.

For two-parallel-CMG system as shown in Fig. 1 and Eq. (1), the angular momentum of the CMG array is constrained in the X–Y plane in the body frame. Then the angular momentum envelope of the CMG array expressed in the body frame can be obtained as:

$$\mathrm{ENV}(\boldsymbol{h}) = \left\{\boldsymbol{h} | h_x^2 + h_y^2 = 4h_0^2, h_z = 0\right\} \tag{12}$$

It should be noted that the body frame coincides with inertial frame when the attitude stabilization is completed. Then the angular momentum envelope expressed in $\mathcal{F}_B$ and $\mathcal{F}_I$ is the same at $t = t_f$ and it is expressed by Eq. (12).

According to Bhat's controllability theory, the angular momentum of the CMG-spacecraft system is controlled at the same angular momentum level determined by the initial condition. Thus the following two conditions should be guaranteed for the attitude control problem using CMGs:

$$\boldsymbol{H}_{\mathcal{F}_I} = \boldsymbol{R}^T(\boldsymbol{J}\boldsymbol{\omega} + \boldsymbol{h}) \equiv \mathrm{Const} \tag{13}$$

$$\boldsymbol{H}_{\mathcal{F}_I} \subset \mathrm{ENV}(\boldsymbol{h})_{\mathcal{F}_I} \tag{14}$$

with ENV $(\boldsymbol{h})_{\mathcal{F}_I}$ representing the momentum envelope of the CMGs in $\mathcal{F}_I$. For Eqs. (13) and (14), Eq. (13) states that the total angular momentum of the whole system is conserved in the inertial frame $\mathcal{F}_I$ when momentum exchange devices are employed as actuators, and Eq. (14) states the controllability as in [13].

Hughes analyzed this problem and gave three different cases, namely, gyrostat with nonspinning carrier (case A), zero momentum gyrostat (case B), and general case (case C) as in [23]. For case A, Bhat's condition is naturally satisfied because the total angular momentum of the CMG-spacecraft system equals to that of the CMG array. Most of the conventional design for an underactuated system concentrates on investigating case B, where the total angular momentum of the CMG-spacecraft system (i.e., $\boldsymbol{H}_t = \boldsymbol{J}\boldsymbol{\omega} + \boldsymbol{h}$) is required to be zero as in [19,20,24–26]. In these references, $\omega_z(t_0)$ about the underactuated axis is always assumed to be zero to satisfy the zero total angular momentum requirement $\boldsymbol{H}_t(t_0) = 0$. Thus Eq. (14) holds regardless of the attitude, and we can always find a proper combination of gimbal angles such that the total angular momentum is equal to zero. However, this is only a subset of the null space of $\boldsymbol{R}^T$ regardless of the attitude $\boldsymbol{Q}$. In addition to this situation, there are some other combinations of $\boldsymbol{Q}$ and $\boldsymbol{\omega}$ such that the Z component of $\boldsymbol{R}^T(\boldsymbol{J}\boldsymbol{\omega} + \boldsymbol{h})$, corresponding to the underacted Z axis, equals zero; that is, $\boldsymbol{H}_{\mathcal{F}_I,z} = [\boldsymbol{R}(\boldsymbol{Q}_0)^T(\boldsymbol{J}\boldsymbol{\omega}(t_0) + \boldsymbol{h}(t_0))]_z = 0$. Then the angular velocity of the spacecraft about Z axis can be possibly damped. Different from most of the existing literature, a more general case where $[\boldsymbol{R}(\boldsymbol{Q}_0)^T(\boldsymbol{J}\boldsymbol{\omega}(t_0) + \boldsymbol{h}(t_0))]_z = 0$ is required rather than $\boldsymbol{J}\boldsymbol{\omega}(t_0) + \boldsymbol{h}(t_0) = 0$. We derive a controller, that is, Eq. (15) of this paper, to achieve a complete attitude stabilization

Table 1 Different initial conditions

Case number	Condition
Case I	$\boldsymbol{H}_t = 0$
Case II	$\boldsymbol{H}_t \neq 0, \boldsymbol{H}_{\mathcal{F}_I,z} = 0$
Case III	$\boldsymbol{H}_{\mathcal{F}_I,z} \neq 0$

when Bhat's controllability condition is satisfied for this general case. Different scenarios are listed in Table 1.

To qualitatively describe the controllability of different scenarios, the angular momentum envelope of the CMG array and the initial angular momentum of the listed three scenarios expressed in $\mathcal{F}_I$ are shown in Fig. 3.

In Fig. 3, the planar ellipse located in the X_I–Y_I plane represents the angular momentum envelope of the two parallel CMGs. This momentum envelope in spacecraft frame wobbles around as the spacecraft attitude changes with time although the angular momentum of the CMG-spacecraft system is conserved in $\mathcal{F}_I$. To guarantee that the spacecraft can be stabilized, the constraints to the initial states should be satisfied. When the system is stabilized, namely, $\boldsymbol{R}(\boldsymbol{Q}_f) = \boldsymbol{I}_3$ and $\mathcal{F}_I$ coincides with $\mathcal{F}_B$ at $t = t_f$, the ellipse is constrained in the X_I–Y_I plane in $\mathcal{F}_I$ the same as in $\mathcal{F}_B$. Case I with $\boldsymbol{H}_t = 0$ shows that the total angular momentum is at the origin. It is obvious that this case is only a small part within the envelope. Except $\boldsymbol{H}_t = 0$, case II with $\boldsymbol{H}_t \neq 0$ and $\boldsymbol{H}_{\mathcal{F}_I,z} = 0$ is also controllable when the angular momentum of the CMG-spacecraft is within the momentum envelope of the CMG array. When the angular momentum of the CMG-spacecraft system belongs to case I or case II, the angular momentum of the spacecraft alone can be absorbed by the actuators. However, when the total angular momentum extends beyond the envelope either along the Z_I axis or in the X_I–Y_I plane, or both, there always exists a component that cannot be influenced through momentum exchange. Then the angular velocity cannot be completely damped. The situations where the complete attitude stabilization is not possible may be the situation as in case III, where the angular momentum has a component sticking out of the planar ellipse in the X_I–Y_I plane, as shown in Fig. 3, or some other cases when the magnitude of $\boldsymbol{H}_t$ is larger than the maximum achievable magnitude of the CMGs' angular momentum even though $\boldsymbol{H}_t$ lies in the X_I–Y_I plane.

III. Inertial Pointing Controller Design

As stated in the system controllability analysis, conventional approaches assume $\boldsymbol{H}_t = 0$. Under this sufficient condition, complete attitude stabilization is achievable. In these studies [19,20,24–26], the Z axis is always assumed to be underactuated, and hence ω_z is assumed to be zero to satisfy the zero total angular momentum requirement. In this paper, the assumption of zero total angular momentum is relaxed. We developed a new controller consisting of two parts, that is, a higher level sliding mode control part $\boldsymbol{\tau}_s$ to stabilize the angular velocity about the underactuated axis (i.e., Z axis) in finite time and a tracking control part $\boldsymbol{\tau}_{tr}$ to track desired angular velocities ω_{dx} and ω_{dy} about the actuated axes (i.e., X axis and Y axis), to achieve complete attitude stabilization. The proposed controller can be written as:

$$\boldsymbol{\tau} = \boldsymbol{\tau}_s + \boldsymbol{\tau}_{tr} \tag{15}$$

with $\boldsymbol{\tau}_s$ stabilizing ω_z and $\boldsymbol{\tau}_{tr}$ stabilizing the remaining five states, ω_x, ω_y, q_1, q_2, and q_3, simultaneously.

In Sec. III.A, desired angular velocities about X (ω_{dx}) and Y (ω_{dy}) axes are specified to control the spacecraft attitude considering the desired angular velocity about Z axis (ω_{dz}) as null. To track these ideal angular velocities about X and Y axes, a feedback controller with feed-forward compensation is designed in Sec. III.B. Section III.C proposes a sliding mode controller to stabilize ω_z in finite time.

A. X-Axis and Y-Axis Rate Commands

In this section, the rate commands to stabilize the kinematics are developed. Separating the angular velocities according to whether the axis is actuated directly by the actuator, kinematics (6) is further rewritten as:

$$\begin{bmatrix} \dot{q}_0 \\ \dot{q}_1 \\ \dot{q}_2 \\ \dot{q}_3 \end{bmatrix} = \frac{1}{2}\begin{bmatrix} -q_1 & -q_2 \\ q_0 & -q_3 \\ q_3 & q_0 \\ -q_2 & q_1 \end{bmatrix}\begin{bmatrix} \omega_{dx} \\ \omega_{dy} \end{bmatrix} + \frac{1}{2}\begin{bmatrix} -q_3 \\ q_2 \\ -q_1 \\ q_0 \end{bmatrix}[\omega_{dz}] \tag{16}$$

In this subsection, the desired value ω_{dz} is set to be zero and hence the second part on the right side of Eq. (16) disappears. Then a nonsingular discontinuous desired angular velocity given in [27] can be used to stabilize the kinematics, which is given by:

$$\omega_{dx} = \begin{cases} -k_1 q_1 + k_2 \dfrac{q_2 q_3}{\boldsymbol{q}_v^T \boldsymbol{q}_v} & \|\boldsymbol{q}_v\| \neq 0 \\ 0 & \|\boldsymbol{q}_v\| = 0 \end{cases}$$
$$\omega_{dy} = \begin{cases} -k_1 q_2 - k_2 \dfrac{q_1 q_3}{\boldsymbol{q}_v^T \boldsymbol{q}_v} & \|\boldsymbol{q}_v\| \neq 0 \\ 0 & \|\boldsymbol{q}_v\| = 0 \end{cases} \tag{17}$$

where $k_1 > 0$, $k_2 > 0$, and $k_2 > 2k_1$. The interpretation of these two parameters is given in Sec. V.

As stated in [27], the kinematic system can be stabilized by the rate command given by Eq. (17) and $\omega_{dz} = 0$ provided the initial condition of $q_1(0)$ and $q_2(0)$ satisfying $q_1(0)^2 + q_2(0)^2 \neq 0$. The detailed proof can be found in the proof of Theorem 1 in [27].

B. Controller for Tracking X-Axis and Y-Axis Rate Commands

To achieve the desired angular velocities, Eq. (17), an angular velocity tracking controller is designed based on the spacecraft dynamics (5). Consider the components along X and Y axes of Eq. (5), we get:

$$\begin{cases} J_x \dot{\omega}_x = a_1^* + \tau_x \\ J_y \dot{\omega}_y = a_2^* + \tau_y \end{cases} \tag{18}$$

where a_1^* and a_2^* are defined as:

$$a_1^* = (J_y - J_z)\omega_y \omega_z + \omega_z h_y$$
$$a_2^* = (J_z - J_x)\omega_x \omega_z - \omega_z h_x \tag{19}$$

and τ_x and τ_y are the torques to be produced by the CMGs.

Furthermore, we define the angular velocity error:

$$\tilde{\omega}_x = \omega_x - \omega_{dx}, \quad \tilde{\omega}_y = \omega_y - \omega_{dy} \tag{20}$$

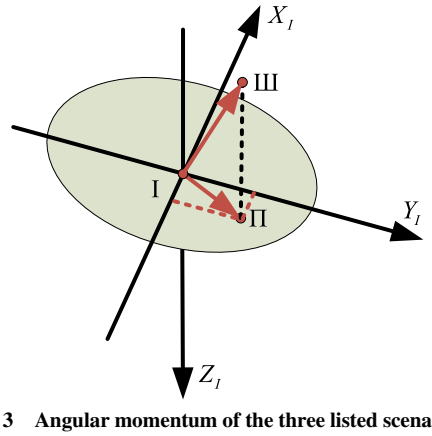

Fig. 3 Angular momentum of the three listed scenarios.

Then we design the angular velocity tracking controller as:

$$\boldsymbol{\tau}_{\text{tr}} = \begin{bmatrix} \tau_{\text{tr}_x} \\ \tau_{\text{tr}_y} \end{bmatrix} = \begin{bmatrix} -a_1^* - k_3 J_x \tilde{\omega}_x + J_x \dot{\omega}_{dx} \\ -a_2^* - k_3 J_y \tilde{\omega}_y + J_y \dot{\omega}_{dy} \end{bmatrix} \tag{21}$$

where k_3 is a positive constant.

Let $\tau_x = \tau_{\text{tr}_x}$ and $\tau_y = \tau_{\text{tr}_y}$ at the velocity tracking stage and substitute the controller (21) into (18). The dynamic system is simplified as:

$$\begin{cases} J_x \dot{\omega}_x = -k_3 J_x \tilde{\omega}_x + J_x \dot{\omega}_{dx} \\ J_y \dot{\omega}_y = -k_3 J_y \tilde{\omega}_y + J_y \dot{\omega}_{dy} \end{cases} \tag{22}$$

The stability can be proved by choosing a Lyapunov function $V_1 = (1/2)\tilde{\boldsymbol{\omega}}^T \bar{\boldsymbol{J}} \tilde{\boldsymbol{\omega}}$ with $\tilde{\boldsymbol{\omega}} = [\tilde{\omega}_x \quad \tilde{\omega}_y]^T$ and $\bar{\boldsymbol{J}} = \text{diag}([J_x \quad J_y])$. Then we can easily obtain $V_1(t) = V_1(0)e^{-2k_3 t}$, and $V_1(t) \to 0$ as $t \to \infty$. Then $\tilde{\boldsymbol{\omega}} \to 0$ implies $\omega_x \to \omega_{dx}$ and $\omega_y \to \omega_{dy}$.

Remark 1: In this subsection, only *X* axis and *Y* axis are controlled to track the desired rate commands. In the following Sec. III.C, a sliding mode controller is designed to track the desired $w_{dz} = 0$ (i.e., ω_z stabilization).

C. ω_z Stabilization Controller

For the underactuated *Z* axis, although ω_z cannot be controlled directly by a torque about the *Z* axis, as there is no actuator to produce a *Z* torque, it can be controlled through its nonlinear coupling with the transverse rates ω_x and ω_y and through the coupling effect produced by the CMG momentum h_x and h_y as shown in Eq. (5). To stabilize ω_z, a sliding mode surface is designed as a linear combination of ω_z and $\dot{\omega}_z$:

$$s = k_4 \omega_z + k_5 \dot{\omega}_z \tag{23}$$

where $k_4 > 0$ and $k_5 > 0$. We also introduce the following notations: $\alpha_1 = 1/J_x, \alpha_2 = 1/J_y, \alpha_3 = 1/J_z$, and $c = (J_x - J_y)/J_z$ to simplify the derivation. Using these notations, dynamics (5) is simplified to:

$$\begin{cases} \dot{\omega}_x = \alpha_1 a_1^* + \alpha_1 \tau_x, \\ \dot{\omega}_y = \alpha_2 a_2^* + \alpha_2 \tau_y, \\ \dot{\omega}_z = c\omega_x \omega_y + \alpha_3 \omega_y h_x - \alpha_3 \omega_x h_y \end{cases} \tag{24}$$

Taking time derivative of the *Z* component of Eq. (24), we obtain:

$$\ddot{\omega}_z = c\dot{\omega}_x \omega_y + c\omega_x \dot{\omega}_y + \alpha_3 \dot{\omega}_y h_x + \alpha_3 \omega_y \dot{h}_x - \alpha_3 \dot{\omega}_x h_y - \alpha_3 \omega_x \dot{h}_y \tag{25}$$

According to the momentum exchange principle $\tau_x = -\dot{h}_x$ and $\tau_y = -\dot{h}_y$, Eq. (25) is further rewritten as:

$$\ddot{\omega}_z = c\dot{\omega}_x \omega_y + c\omega_x \dot{\omega}_y + \alpha_3 \dot{\omega}_y h_x - \alpha_3 \dot{\omega}_x h_y - \alpha_3 \omega_y \tau_x + \alpha_3 \omega_x \tau_y \tag{26}$$

Thus the time derivative of *s* can be obtained as:

$$\begin{aligned} \dot{s} &= k_4 \dot{\omega}_z + k_5 \ddot{\omega}_z \\ &= k_4 (c\omega_x \omega_y + \alpha_3 \omega_y h_x - \alpha_3 \omega_x h_y) \\ &\quad + k_5 (c\dot{\omega}_x \omega_y + c\omega_x \dot{\omega}_y + \alpha_3 \dot{\omega}_y h_x - \alpha_3 \dot{\omega}_x h_y - \alpha_3 \omega_y \tau_x + \alpha_3 \omega_x \tau_y) \end{aligned} \tag{27}$$

Substituting $\dot{\omega}_x, \dot{\omega}_y$ from Eq. (24), controller (15), and $\boldsymbol{\tau}_{\text{tr}}$, Eq. (20), in Eq. (27), we obtain:

$$\dot{s} = \boldsymbol{\Lambda}^T \boldsymbol{\tau}_s + \Phi(\bullet) \tag{28}$$

with Λ, $\Phi(\bullet)$ defined as:

$$\boldsymbol{\Lambda} = k_5 \begin{bmatrix} (c\alpha_1 - \alpha_3)\omega_y - \alpha_3 \alpha_1 h_y \\ (c\alpha_2 + \alpha_3)\omega_x + \alpha_3 \alpha_2 h_x \end{bmatrix} \tag{29}$$

$$\begin{aligned} \Phi(\bullet) = {} & ck_4 \omega_x \omega_y + \alpha_3 k_4 h_x \omega_y - \alpha_3 k_4 h_y \omega_x - ck_3 k_5 \tilde{\omega}_x \omega_y \\ & - ck_3 k_5 \tilde{\omega}_y \omega_x + ck_5 \dot{\omega}_{dx} \omega_y + ck_5 \dot{\omega}_{dy} \omega_x - \alpha_3 k_3 k_5 \tilde{\omega}_y h_x \\ & + \alpha_3 k_3 k_5 \tilde{\omega}_x h_y + \alpha_3 k_5 \dot{\omega}_{dy} h_x - \alpha_3 k_5 \dot{\omega}_{dx} h_y - \alpha_3 k_5 J_x \omega_y \dot{\omega}_{dx} \\ & + \alpha_3 k_3 k_5 J_x \omega_y \tilde{\omega}_x + \alpha_3 k_5 J_y \omega_x \dot{\omega}_{dy} - \alpha_3 k_3 k_5 J_y \omega_x \tilde{\omega}_y \\ & + \alpha_3 a_1^* k_5 \omega_y - \alpha_3 a_2^* k_5 \omega_x \end{aligned} \tag{30}$$

Then, to stabilize ω_z, the sliding mode control term $\boldsymbol{\tau}_s$ is designed as:

$$\boldsymbol{\tau}_s = -\big(k_6 s + k_7 \text{sgn}(s)\big)\boldsymbol{\Lambda}^+ \tag{31}$$

where $k_6 > 0$, $k_7 = \|\Phi(\bullet)\| + k_8$, $k_8 > 0$, and the operator $\boldsymbol{x}^+$ is given by:

$$\boldsymbol{x}^+ = \begin{cases} \dfrac{\boldsymbol{x}}{\boldsymbol{x}^T \boldsymbol{x}} & \|\boldsymbol{x}\| \neq 0 \\ \boldsymbol{0} & \|\boldsymbol{x}\| = 0 \end{cases} \tag{32}$$

Thus the overall control law (15) can be written as:

$$\boldsymbol{\tau} = -\big(k_6 s + k_7 \text{sgn}(s)\big)\boldsymbol{\Lambda}^+ + \begin{bmatrix} -a_1^* + J_x \dot{\omega}_{dx} - k_3 J_x \tilde{\omega}_x \\ -a_2^* + J_y \dot{\omega}_{dy} - k_3 J_y \tilde{\omega}_y \end{bmatrix} \tag{33}$$

Now we proceed to prove the stability using the Lyapunov approach. A Lyapunov function is chosen as:

$$V_2 = \frac{s^2}{2} \tag{34}$$

The time derivation of the Lyapunov function is:

$$\dot{V}_2 = s\dot{s} \tag{35}$$

Substituting the controller (31) and (28) into Eq. (35):

$$\begin{aligned} \dot{V}_2 = s\dot{s} &= s\big[\boldsymbol{\Lambda}^T \boldsymbol{\tau}_s + \Phi(\bullet)\big] \\ &= s\big[-k_6 s \boldsymbol{\Lambda}^T \boldsymbol{\Lambda}^+\big] - s\big[k_7 \text{sgn}(s) + \Phi(\bullet)\big] \\ &\leq -k_6 s^2 - k_8 |s| = -2k_6 V_2 - 2k_8 \sqrt{V_2} \leq 0 \end{aligned} \tag{36}$$

Thus $V_2 \leq V_2(0)e^{-2k_6 t}$, and V_2 reaches zero in finite time $T \leq (1/k_6)\,\ell_n((\sqrt{2}k_6 \sqrt{V_2(s(t_0))} + k_8)/k_8)$ [28,29]. When $t > T$, $s = 0$, $\omega_z = \omega_{dz} = 0$ is achieved. The controller (33) is reduced to Eq. (21), and the desired angular velocities can be tracked. Thus, the complete kinematics can be stabilized as per Remark 1.

In summary, the whole design process can be concluded by the following theorem:

Theorem 1: Consider the underactuated spacecraft with two parallel SGCMGs as in Fig. 1; a complete attitude stabilization of the dynamic system (5) and kinematics (6) can be achieved by controller (33) when the angular momentum of the spacecraft-CMG system lies within the momentum envelope of the CMG array. □

To improve the control performance, a smooth hyperbolic tangent function is employed to approximate the discontinuous signum function as:

$$\boldsymbol{\tau} = -\big(k_6 s + k_7 \tanh(s)\big)\boldsymbol{\Lambda}^* + \begin{bmatrix} -a_1^* + J_x\dot{\omega}_{dx} - k_3 J_x \tilde{\omega}_x \\ -a_2^* + J_y\dot{\omega}_{dy} - k_3 J_y \tilde{\omega}_y \end{bmatrix} \tag{37}$$

with

$$\boldsymbol{\Lambda}^* = \frac{\boldsymbol{\Lambda}}{\boldsymbol{\Lambda}^T\boldsymbol{\Lambda} + |s|} \tag{38}$$

We will use the controller (37) in the numerical simulation, which results in an acceptable performance though the strict proof using the smooth hyperbolic tangent function is not given.

IV. Singularity and Steering Laws

We employ two parallel CMGs as the actuators. The control command generated by the controller should be realized by the actuators. Then the steering law is needed to compute the gimbal angular rate in response to the control command. However, the Jacobian matrix $\boldsymbol{A}$ may lose rank and physically the output torques may align, which would lead to a singularity.

A. Singularity of the Two Parallel CMGs

The Jacobian matrix $\boldsymbol{A}$ is invertible except for some singularity conditions. Calculating the determinant of the matrix $\boldsymbol{A}$, we obtain:

$$\det(\boldsymbol{A}) = \sin\delta_2\cos\delta_1 - \sin\delta_1\cos\delta_2 = \sin(\delta_2 - \delta_1) \tag{39}$$

It is clear that matrix $\boldsymbol{A}$ loses rank when:

$$\delta_2 - \delta_1 = k\pi (k \in \mathbb{Z}) \tag{40}$$

where $\mathbb{Z}$ is the set of integers.

Correspondingly, the singularity may be either internal or external, as shown in Fig. 4.

For the case shown in Fig. 4a with $k = (2n+1)(n \in \mathbb{Z})$, the singularity is internal. The output torques of these two CMGs will be antiparallel, namely, $\tau_2 = -\tau_1$. Then the overall output torque will be zero and the spacecraft will be uncontrollable at this time instant. For the case shown in Fig. 4b, $k = 2n(n \in \mathbb{Z})$. τ_1 and τ_2 are in the same direction and cannot generate an orthogonal component. The CMG array generates the maximum control torque, and no additional torque can be produced. This singularity is called the external singularity.

B. Modified Inverse Steering Law

To map the 2-dimensional orthogonal control torque to the two gimbal angular rates, the inverse of the Jacobian matrix is needed. There are various steering laws, such as singularity avoidance steering law, singularity escape steering law, and the hybrid logic [10,11]. For the 2×2 matrix $\boldsymbol{A}$ as in this paper, the adjoint matrix is easy to obtain, and so we will simply invert the 2×2 matrix $\boldsymbol{A}$.

If $\det(\boldsymbol{A}) \neq 0$, we can easily obtain:

$$\boldsymbol{A}^{-1} = \frac{1}{\det(\boldsymbol{A})}\begin{bmatrix} \cos\delta_2 & \sin\delta_2 \\ -\cos\delta_1 & -\sin\delta_1 \end{bmatrix} \tag{41}$$

However, Eq. (39) states that $\det(\boldsymbol{A})$ goes to zero under the condition of Eq. (40). To avoid the difficulty in calculating $\boldsymbol{A}^{-1}$ via Eq. (40), a small positive angle δ_e is added in calculating the determinant while the real gimbal angles are not changed:

$$\det(\boldsymbol{A}) = \sin(\delta_2 - \delta_1 + \delta_e) \quad (|\sin(\delta_2 - \delta_1)| < \varrho, \varrho > 0) \tag{42}$$

To guarantee the singularity escaping by this modification, δ_e and ϱ should satisfy:

$$\delta_e > 2\arcsin\varrho \tag{43}$$

which means that $\det(\boldsymbol{A}) > \varrho$ after the modification.

Then $(\det \boldsymbol{A})^*$ is denoted as:

$$(\det \boldsymbol{A})^* = \begin{cases} \sin(\delta_2 - \delta_1) & |\sin(\delta_2 - \delta_1)| \geq \varrho \\ \sin(\delta_2 - \delta_1 + \delta_e) & |\sin(\delta_2 - \delta_1)| < \varrho \end{cases} \tag{44}$$

and $\det(\boldsymbol{A})$ in Eq. (39) is replaced with $(\det \boldsymbol{A})^*$ to generate $\boldsymbol{A}^{-1}$ with the cost of introducing a torque error.

According to Eq. (2), when $\boldsymbol{\tau}_c = \boldsymbol{\tau}$, the gimbal rates can be generated via:

$$\dot{\boldsymbol{\delta}} = -\frac{1}{h_0}\boldsymbol{A}^{-1}\boldsymbol{\tau} \tag{45}$$

C. Comparison of the Steering Laws

The effectiveness of the proposed modified inverse (MI) steering law is shown in this section and it is compared with the generalized singular robust (GSR) inverse logic [9,22]. The GSR for a 2×2 Jacobian matrix $\boldsymbol{A}$ can be given by:

$$\dot{\boldsymbol{\delta}} = -\frac{1}{h_0}\boldsymbol{A}^{\#}\boldsymbol{\tau} \quad \text{where } \boldsymbol{A}^{\#} = \boldsymbol{A}^T(\boldsymbol{A}\boldsymbol{A}^T + \lambda\boldsymbol{E})^{-1} \tag{46}$$

and

$$E = \begin{bmatrix} 1 & \varepsilon \\ \varepsilon & 1 \end{bmatrix} > 0, \quad \varepsilon = \varepsilon_0\sin(\omega t + \phi), \quad \lambda = \lambda_0 e^{-\mu\det(AA^T)}$$

with ε_0, ω, ϕ, λ_0, and μ are all positive numbers and the possible values can be found in [22].

To quantitatively measure the torque error generated by the steering law, we define an index:

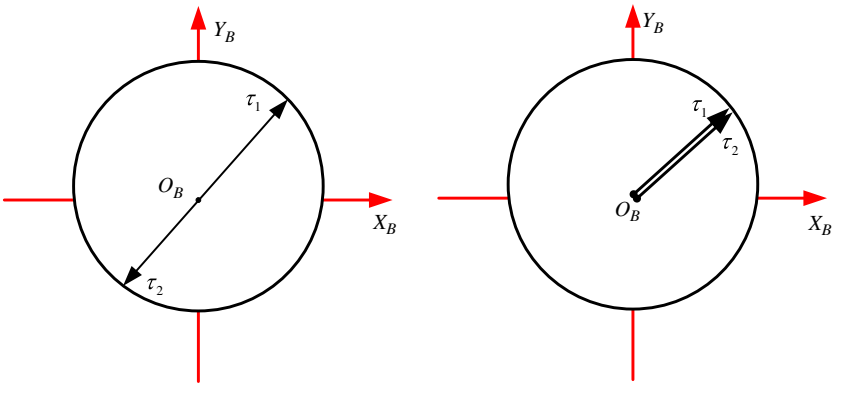

a) Internal singularity b) External singularity

Fig. 4 Singularity of the two-parallel-CMG configuration.

$$\kappa = \int \boldsymbol{\tau}_e^T \boldsymbol{\tau}_e \, \mathrm{d}t \tag{47}$$

where $\boldsymbol{\tau}_e$ is the difference between the torque generated by the actuators and the torque required by the controller.

In this section, we choose the same parameters as in [22], namely: $\lambda_0 = 0.01$, $\mu = 10$, $\varepsilon = 0.01\sin(0.05\pi t + 0.5\pi)$. For the steering law of Eq. (42), ϱ is chosen to be 0.001, then we have $\arcsin\varrho = 0.0573°$, and so δ_e is chosen to be 0.12 deg. The control command is set to be $\tau_x = 0.05\sin(0.05\pi t)$ N · m and $\tau_y = 0.05\cos(0.05\pi t)$ N · m.

Case I: $\delta_1 = \delta_2 = 0$

According to Eq. (40), the initial angles would represent externally singular configuration. This case is to show the effectiveness of singularity escaping. The results are shown in Fig. 5. It can be seen from Fig. 5a that the gimbal angles are steered out of the singular domain immediately using the proposed MI method. However, the singular measure of the GSR is quite close to zero. The torque error measurement index κ is shown in Fig. 5b. It can been seen that, for the MI steering law, the torque error integral remains small after exiting from the singularity. On the contrary, when GSR is applied, the torque error exists during the whole simulation process and the torque error integral κ increases gradually. So we can conclude that the MI steering law is more effective in escaping singularity and more precise in torque generation compared with the GSR in this simulation when the initial gimbals are in external singularity configuration, that is, when the CMG momentums are parallel, as in Fig. 4b.

Case II: $\delta_1 = 0, \delta_2 = 0.5\pi$

Figure 6 compares the two steering laws when the initial gimbal angles are nonsingular. Figure 6a demonstrates that the singularity measures of the two steering laws are similar. The gimbal angles enter singularity around $t = 10$ s and leave singularity soon. Besides, the magnitude of the torque error using MI is smaller than the magnitude with GSR according to the simulation results.

We note that the performance of GSR depends highly on the parameters ε_0, ϵ, λ_0, and μ. If some optimal values are chosen, the performance may improve. However, the torque error exists during the whole process because of the synthesis of the time-varying perturbed matrix $\lambda \boldsymbol{E}$ to escape singularity. Compared with GSR, the MI method requires only a small modification at the singular time instant. Thus the overall torque error is potentially expected to be smaller than that with GSR. Another advantage of MI is the simplicity in calculation. For MI in dealing with two SGCMGs, the inverse of the Jacobian matrix is given by an analytic Eq. (41) and the calculation of time varying matrix $\lambda \boldsymbol{E}$ is removed.

Remark 2: The proposed MI method is developed for the two-SGCMG system, and the conclusions made above are only for this situation. For other cases when the number of SGCMG is greater than 2, GSR is still a good choice when MI is not applicable.

V. Numerical Simulation

In this section, numerical examples are illustrated using the proposed attitude stabilization controller (37) and the CMG steering law (39–45). The spacecraft is chosen as the 320 kg minisatellite

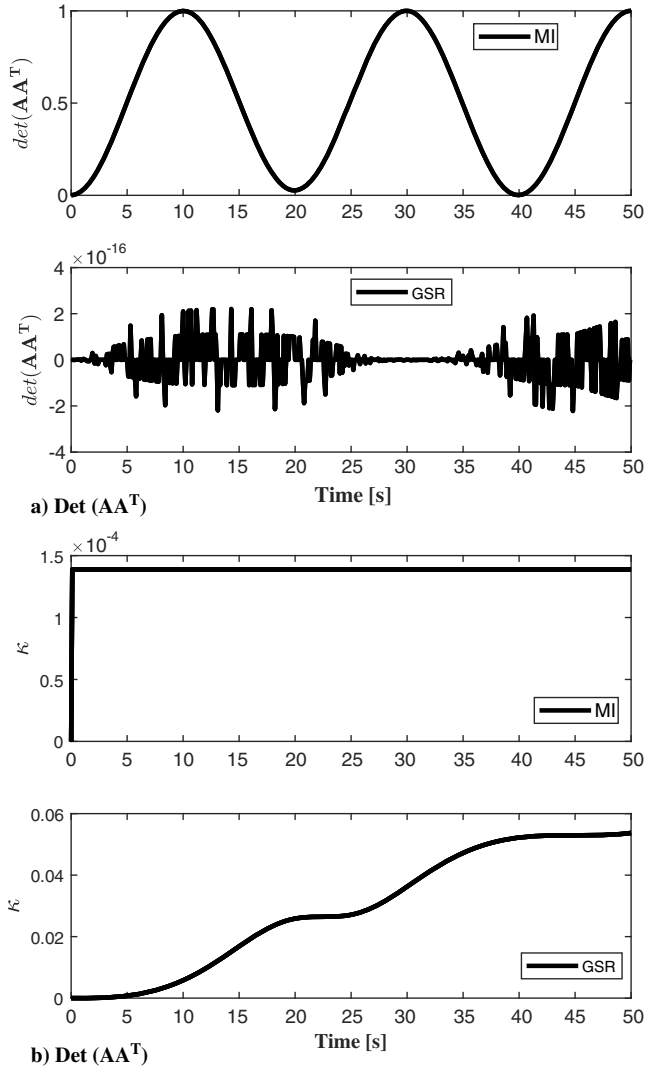

Fig. 5 Steering law comparison with initial angles from singularity domain.

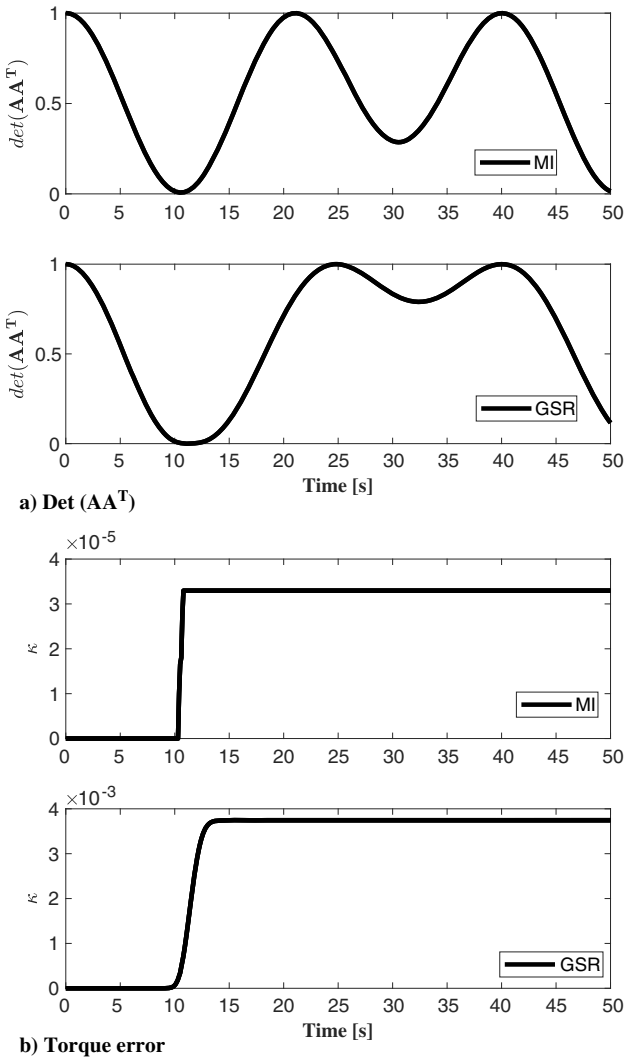

Fig. 6 Steering law comparison with initial angles from nonsingularity domain.

Uosat-12 as in [25]. The moments of inertia of the principle axes are:

$$J_x = 40.45, \quad J_y = 42.09, \quad J_z = 42.36 \text{ kg} \cdot \text{m}^2$$

For the CMGs, [30,31] furnish parameters of a micro-CMG, with the angular momentum h_0 being 0.23 and 0.28 N · m · s for a 130 kg satellite BILSAT-1. Then we can choose the ideal value $h_0 = 0.347$ N · m · s as in [30] for this 320 kg minisatellite. The maximum gimbal angular velocity is set to be 60 deg /s.

In the simulation, k_1 is the slope of the linear switching line in the $\boldsymbol{\omega} - \boldsymbol{q}_v$ plane (similar to the phase plane), and k_2 is a gain for the nonlinear term in Eq. (17). They are chosen as $k_1 = 0.01$, $k_2 = 0.08$ as in [25]. k_3 is the inverse of the time constant of the rate error control; see Eqs. (21) and (22). It is chosen as $1/k_3 = 20$ s. k_4 and k_5 appear in the sliding mode surface for ω_z and $\dot{\omega}_z$; see Eq. (23). These two parameters, k_4 and k_5, are used to govern the system performance on the sliding surface and they are chosen as $k_4 = 11$ and $k_5 = 1$, respectively. k_6 and $k_7 (k_7 = \|\Phi\| + k_8)$ are the feedback gains of s and sign (s) to guarantee the finite time convergence; see Eq. (31).

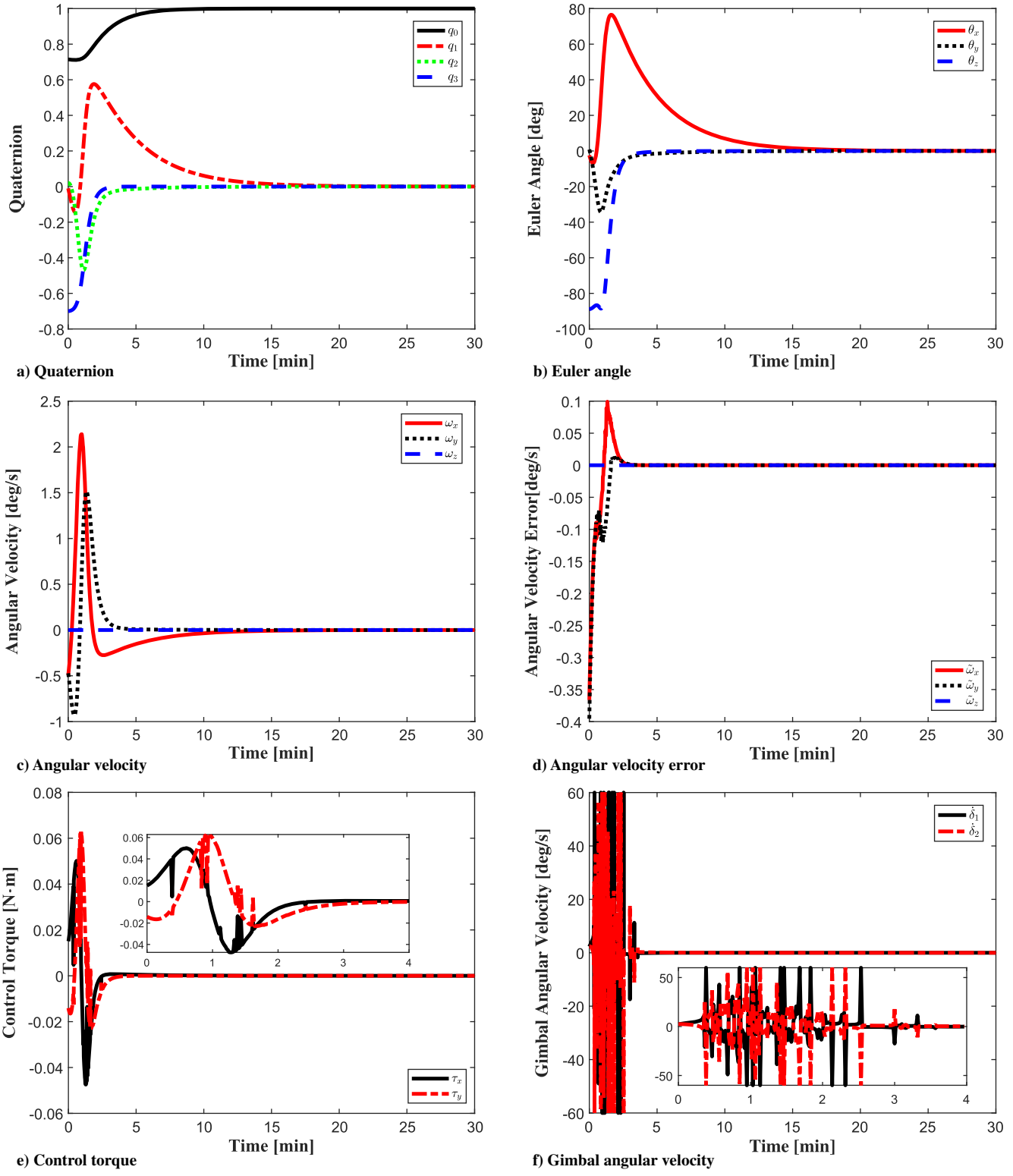

Fig. 7 Control results of case I ($H_t = 0$).

Thus k_6 and k_8 are used to govern the transients of controlling the Z component of the angular rate ω_z, and are chosen to be $k_6 = 4$ and $k_8 = 0.1$.

Remark 3: The control performance depends highly on the parameters in the controller, and convergence time increases with improper gains. How to choose the parameters systematically is still an open problem. In this paper, k_1 and k_2 are chosen according to [23]. k_5 is chosen to be 1 because it will be in the denominator in generating Λ^+. This choice makes it easier to tune the parameters. k_8 is set to be a small value according to the derivation. For other parameters, we first choose a k_3 to get a relative good performance. Then increase k_4 and k_6 to guarantee the convergence of ω_z. Finally k_8 is tuned to get the desired performance.

The simulation results of the three cases pertaining to different initial conditions in Table 1 are shown below:

Case I: $\boldsymbol{H}_t = 0$

In this case, the total momentum of CMG-spacecraft is assumed to be zero. The gimbal angles of the CMGs are set to be $\delta_1 = 0$ and $\delta_2 = \pi/2$. According to Eq. (1), the angular velocities of the spacecraft are set as $\omega_x = -h_0/J_x = -0.4915$ deg /s, $\omega_y = -h_0/J_y = -0.4724$ deg /s and $\omega_z = 0$ deg /s. As mentioned before, $\boldsymbol{H}_t = 0$ is the simplest solution of $\boldsymbol{R}^T\boldsymbol{H}_t = 0$ regardless of the attitude $\boldsymbol{Q}$. Then the initial condition for the quaternion is chosen as $\boldsymbol{q}_v = [-0.01, 0.02, -0.7]^T$, $q_0 = \sqrt{1 - \boldsymbol{q}_v^T\boldsymbol{q}_v} = 0.7138$. The simulations results are shown in Fig. 7.

As shown in Figs. 7a and 7b, the attitude is stabilized within 20 min. Figure 7b shows the Euler angles corresponding to Fig. 7a with a "Z-Y-X" rotation, and it shows that a large-angle ($\theta_x(t_0) \approx -2.4$ deg, $\theta_y(t_0) \approx 0.83$ deg, $\theta_z(t_0) \approx -88.9$ deg) maneuver is completed. It is also noted that θ_x and θ_y increase while controlling θ_z to zero. This is because there is no direct control input on the Z axis, and hence the developed controller renders ω_z and q_3 to zero first via the coupling effect. Figures 7c and 7d demonstrate the angular velocity–related results. It can be concluded from Fig. 7c that the angular velocity converges to zero in about 20 min. The maximum angular velocity error in Fig. 7d is 0.4 deg /s at $t = 0$, and after 5 min when the angular velocity error approaches zero, the angular velocity follows the desired value well. Then the kinematic equations are steered to reach equilibrium by the desired angular velocity as stated in Sec. II.A and Theorem 1 in [27]. Figure 7e portrays the control torque output. The maximum value is smaller than 80 mN · m, which is far below the maximum achievable control torque, $\tau_{\max} = 2h_0\dot{\delta}_{\max} = 2 \times 0.347 \times \pi/3 = 726.38$ mN · m. Figure 7f illustrates the gimbal rate constrained by limit of 60 deg /s. In this case, the total angular momentum is zero, and it corresponds to the origin in both $\mathcal{F}_B$ and $\mathcal{F}_I$.

Case II: $\boldsymbol{H}_t \neq 0$, $\boldsymbol{H}_{\mathcal{F}_I,z} = 0$

In case I, the total angular momentum in $\mathcal{F}_I$ resides in the momentum envelope of the CMGs automatically when $\boldsymbol{H}_t = 0$. There still exists a subset of combinations of the attitude $\boldsymbol{Q}$ and angular velocity $\boldsymbol{\omega}$, making the Z component of $\boldsymbol{H}_{\mathcal{F}_I}$ zero. When $\boldsymbol{Q}$ and $\boldsymbol{\omega}$ are in this subset under the conditions of Eqs. (13) and (14), they can also be stabilized using the proposed controller.

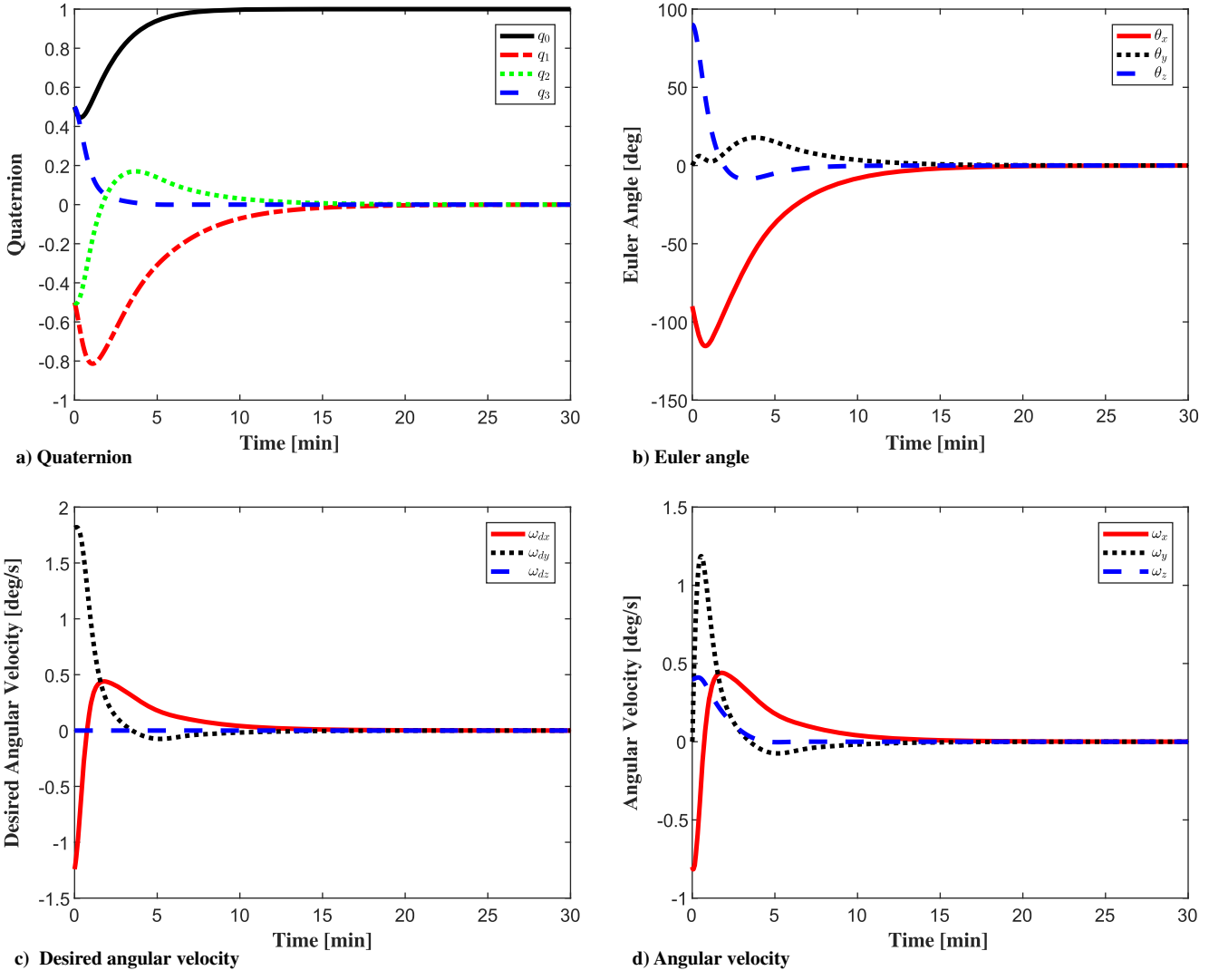

a) Quaternion b) Euler angle

c) Desired angular velocity d) Angular velocity

Fig. 8 Control results of case II ($H_t \neq 0$, $H_{\mathcal{F}_I,z} = 0$): a) quaternion, b) Euler angle, c) desired angular velocity, and d) angular velocity.

Since $\boldsymbol{Q}$ and $\boldsymbol{\omega}$ are dependent in this case as in Eq. (13), we will choose $\boldsymbol{Q}$ first and then choose $\boldsymbol{\omega}$. According to the relationship of $\boldsymbol{R}$ and $\boldsymbol{Q}$, we chose $\boldsymbol{Q} = [0.5, -0.5, -0.5, 0.5]^T$. Then $\boldsymbol{\omega}$ is chosen to be $\omega_x = -0.8$ deg/s, $\omega_y = 0$ deg/s, and $\omega_z = 0.4$ deg/s to guarantee $\boldsymbol{H}_{\mathcal{F}_I,z} = 0$. The gimbal angles are set as $\delta_1 = \delta_2 = 0$ deg. Finally, the total angular momentum in $\mathcal{F}_B$ and $\mathcal{F}_I$ are calculated to be $\boldsymbol{H}_t = [0.1292, 0, 0.2957]^T$ N · m · s and $\boldsymbol{H}_{\mathcal{F}_I} = [-0.2957, 0.1292, 0]^t$ N · m · s, respectively. These initial conditions satisfy the controllability requirement of Eqs. (13) and (14), and attitude stabilization is expected to be achievable.

Figures 8 and 9 show the angular velocity stabilization and attitude stabilization ability with the utilization of controller (37) and the steering logic (39–45). Figures 8a and 8b show the attitude trajectory of the maneuver. It can be seen that the attitude is stabilized in 20 min. More specifically, about 90° maneuver about X and Z axes is completed as shown in Fig. 8b. From the response of desired angular velocity (Fig. 8c), angular velocity (Fig. 8d), and angular velocity error (Fig. 9a), we conclude that the velocities about X and Y axes are controlled to track the desired angular velocity, and the velocity about the Z axis is gradually damped by the coupling control effect. This phenomenon is observed clearly in the angular velocity error of Fig. 9a, which shows that $\tilde{\omega}_x$ and $\tilde{\omega}_y$ converge to zero quickly and $\tilde{\omega}_z$ is stabilized after $\tilde{\omega}_x$ and $\tilde{\omega}_y$ reach zero. Figure 9b shows that the maximum control torque is smaller than 80 mN · m and it is within the limit of the micro-CMG. The trajectory of angular momentum in $\mathcal{F}_B$ is demonstrated in Fig. 9d. It is clear that the total angular momentum in the body frame is not conserved in terms of components, but the magnitude is kept within numerical precision. We also calculated $\boldsymbol{H}_{\mathcal{F}_I}$ and found that it always stays at the initial value. So the figure of $\boldsymbol{H}_{\mathcal{F}_I}$ is not shown here.

Case III: $\boldsymbol{H}_{\mathcal{F}_I,z} \neq 0$

In this case, the initial values are almost the same as in case II except for ω_y. Here we set ω_y to be 0.1 deg/s. Then the total angular momentums in $\mathcal{F}_B$ and $\mathcal{F}_I$ are $\boldsymbol{H}_t = [0.1292, 0.0735, 0.2957]$ N · m · s and $\boldsymbol{H}_{\mathcal{F}_I} = [-0.2957, 0.1292, -0.0735]$ N · m · s, respectively. The constraint of $\boldsymbol{H}_{\mathcal{F}_I,z} = 0$ is not satisfied. It is obvious that the angular velocity about the Z axis in $\mathcal{F}_B$ cannot be absorbed by the actuators. Thus the attitude cannot be completely stabilized. Figure 10 shows the simulation results.

As in the previous analysis, Fig. 10 shows that the angular velocity and attitude cannot be completely stabilized. It can be seen from Fig. 10a that the attitude will be controlled into a small region with periodic oscillations. Figure 10b shows the Z-axis trajectory in the inertial frame. The initial attitude is marked as square and the target is marked as diamond. It is clear that the attitude is controlled to rotate around the target attitude in a small region. Figure 10c demonstrates the history of the angular velocity. The angular velocity is controlled to converge into a region and then it starts to oscillate because of the increase of the desired angular velocity. Figure 10d shows the angular velocity trajectory in the inertial frame. It also shows that the angular velocity oscillates eventually. Figures 10e and 10f show the control torque and gimbal rates. Similar to angular velocity, the angular momentum oscillates in the body frame, whereas it is conserved in the inertial frame.

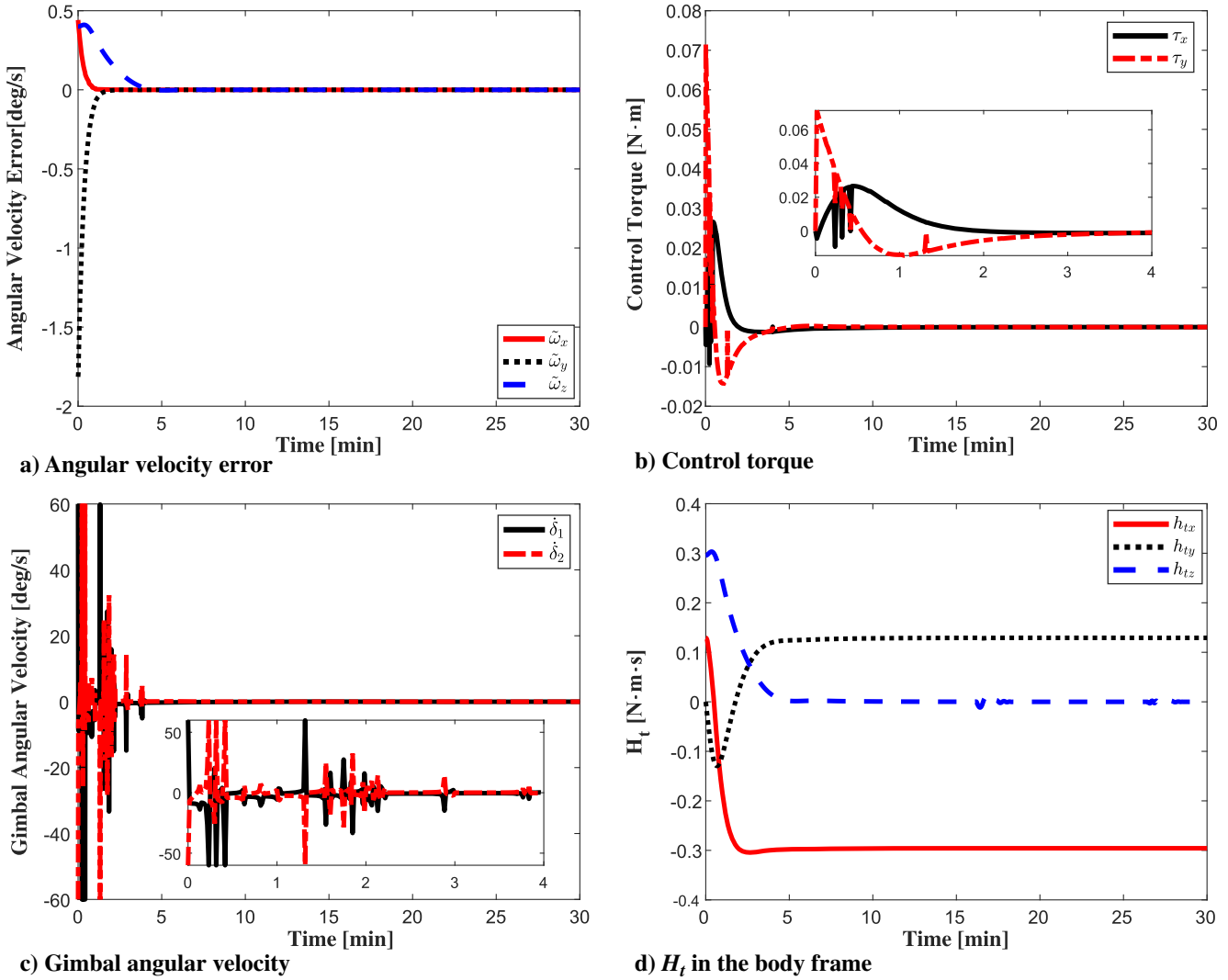

Fig. 9 Control results of case II ($H_t \neq 0$, $H_{\mathcal{F}_I,z} = 0$): a) angular velocity error, b) control torque, c) gimbal angular velocity, and d) H_t.

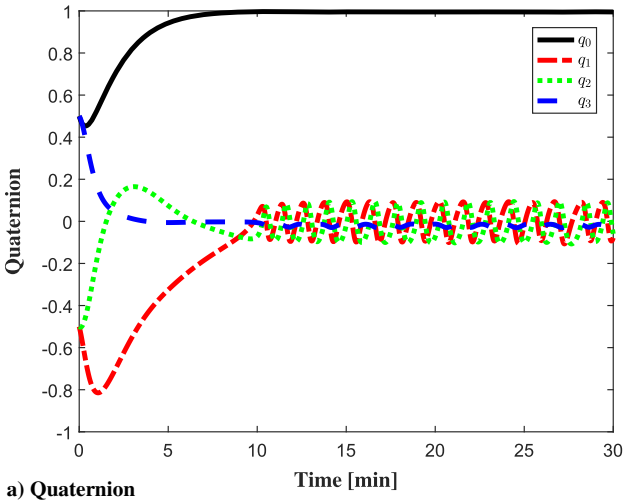

a) Quaternion

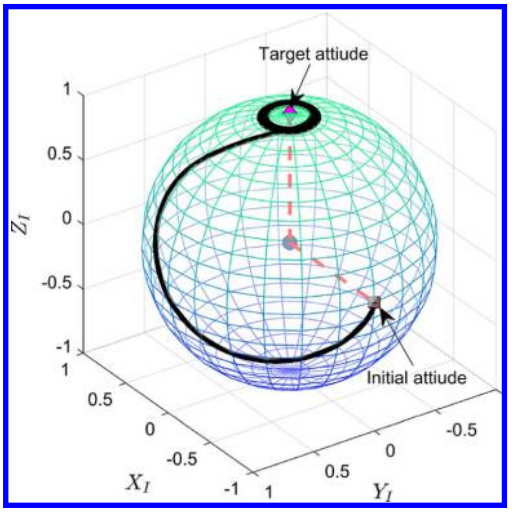

b) Attitude trajectory in inertial frame

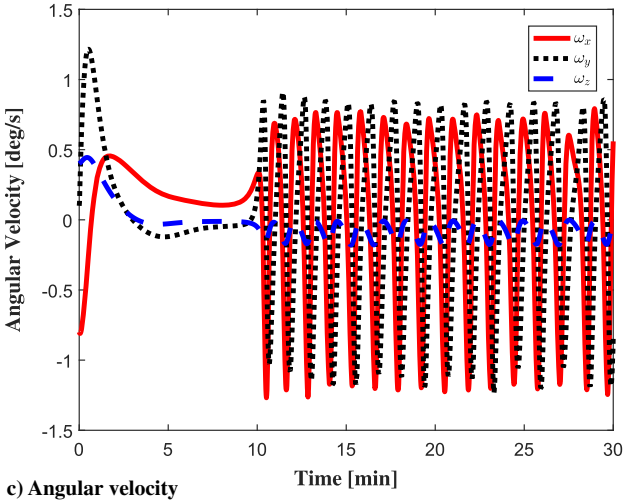

c) Angular velocity

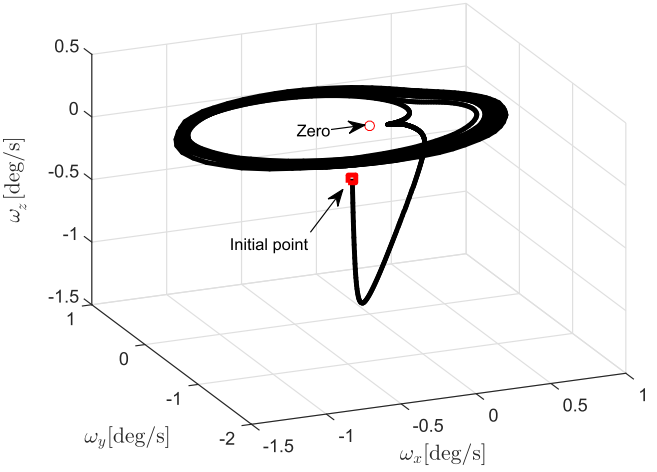

d) Angular velocity in inertial frame

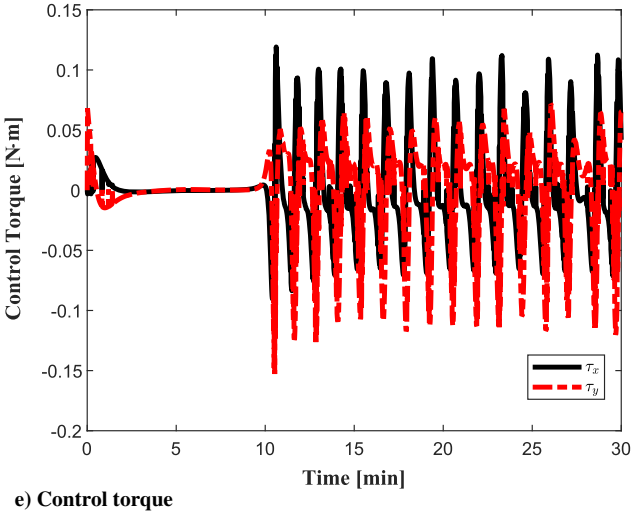

e) Control torque

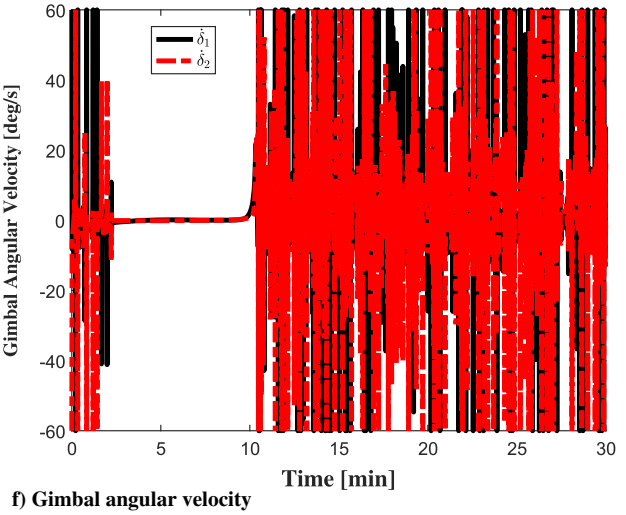

f) Gimbal angular velocity

Fig. 10 Control results of case III ($H_{\mathcal{F}_I,z} \neq 0$).

VI. Conclusions

This paper investigates the underactuated attitude stabilization problem using two parallel control moment gyros without the zero total angular momentum assumption. This control objective is achieved by a joint control strategy containing an angular velocity tracking control term and a sliding mode control term. For the first term, desired rate commands about the actuated axes are designed to stabilize the complete kinematics with zero desired angular velocity about the underactuated axis. Then a rate command tracker is developed to track the designed angular velocities. For the sliding term, the coupling effect of the system dynamics is employed to stabilize the nonzero angular velocity component about the axis

without control input. Then underactuated attitude stabilization is completed. To map the control command into the gimbal angular velocity domain precisely, a steering law with low computation is proposed. Simulation results verify the effectiveness of the proposed controller and steering law.

Acknowledgement

We would like to express our sincere thanks to the editor, associate editor, and reviewers for their patience, time, and effort devoted to reviewing our work and making it publishable.

References

[1] Tafazoli, M., "A Study of On-Orbit Spacecraft Failures," *Acta Astronautica*, Vol. 64, No. 2, 2009, pp. 195–205. doi:10.1016/j.actaastro.2008.07.019

[2] Petersen, C. D., Leve, F., and Kolmanovsky, I., "Underactuated Spacecraft Switching Law for Two Reaction Wheels and Constant Angular Momentum," *Journal of Guidance, Control, and Dynamics*, Vol. 39, No. 9, 2016, pp. 2086–2099. doi:10.2514/1.G001680

[3] Xiao, B., Hu, Q. L., Singhose, W., et al., "Reaction Wheel Fault Compensation and Disturbance Rejection for Spacecraft Attitude Tracking," *Journal of Guidance, Control, and Dynamics*, Vol. 36, No. 6, 2013, pp. 1565–1575. doi:10.2514/1.59839

[4] Shen, Q., Wang, D. W., Zhu, S. Q., et al., "Robust Control Allocation for Spacecraft Attitude Tracking Under Actuator Faults," *IEEE Transactions on Control Systems Technology*, Vol. 25, No. 3, 2017, pp. 1068–1075. doi:10.1109/TCST.2016.2574763

[5] Hill, D. E., "Dynamics and Control of Spacecraft Using Control Moment Gyros with Friction Compensation," *Journal of Guidance, Control, and Dynamics*, Vol. 39, No. 10, 2016, pp. 2406–2418. doi:10.2514/1.G001585

[6] Bedrossian, N. S., Paradiso, J., Bergmann, E. V., et al., "Redundant Single Gimbal Control Moment Gyroscope Singularity Analysis," *Journal of Guidance, Control, and Dynamics*, Vol. 13, No. 6, 1990, pp. 1096–1101. doi:10.2514/3.20584

[7] Wie, B., "Singularity Analysis and Visualization for Single-Gimbal Control Moment Gyro Systems," *Journal of Guidance, Control, and Dynamics*, Vol. 27, No. 2, 2004, pp. 271–282. doi:10.2514/1.9167

[8] Yang, Y., "Singularity-Free Model Predictive Spacecraft Attitude Regulation Using a Variable-Speed Control Moment Gyroscopes Model," *IEEE Transactions on Aerospace and Electronic Systems*, Vol. 54, No. 3, 2017, pp. 1511–1518. doi:10.1109/TAES.2018.2796878

[9] Wie, B., Bailey, D., and Heiberg, C., "Singularity Robust Steering Logic for Redundant Single-Gimbal Control Moment Gyros," *Journal of Guidance, Control, and Dynamics*, Vol. 24, No. 5, 2001, pp. 865–872. doi:10.2514/2.4799

[10] Leve, F. A., and Fitz-Coy, N. G., "Hybrid Steering Logic for Single-Gimbal Control Moment Gyroscopes," *Journal of Guidance, Control, and Dynamics*, Vol. 33, No. 4, 2010, pp. 1202–1212. doi:10.2514/1.46853

[11] Leve, F. A., "Evaluation of Steering Algorithm Optimality for Single-Gimbal Control Moment Gyroscopes," *IEEE Transactions on Control Systems Technology*, Vol. 22, No. 3, 2014, pp. 1130–1134. doi:10.1109/TCST.2013.2259829

[12] Crouch, P., "Spacecraft Attitude Control and Stabilization: Applications of Geometric Control Theory to Rigid Body Models," *IEEE Transactions on Automatic Control*, Vol. 29, No. 4, 1984, pp. 321–331. doi:10.1109/TAC.1984.1103519

[13] Bhat, S. P., and Tiwari, P. K., "Controllability of Spacecraft Attitude Using Control Moment Gyroscopes," *IEEE Transactions on Automatic Control*, Vol. 54, No. 3, 2009, pp. 585–590. doi:10.1109/TAC.2008.2008324

[14] McInnes, C. R., "Gain-Scheduled Control and Singularity Avoidance with a Double-Gimbal Variable-Speed Control Moment Gyro," *AIAA/AAS Astrodynamics Specialist Conference*, AIAA Paper 2016-5370, 2016. doi:10.2514/6.2016-5370

[15] Kasai, S., Kojima, H., and Satoh, M., "Spacecraft Attitude Maneuver Using Two Single-Gimbal Control Moment Gyros," *Acta Astronautica*, Vol. 84, March–April 2013, pp. 88–98. doi:10.1016/j.actaastro.2012.07.035

[16] Kwon, S., Shimomura, T., and Okubo, H., "Pointing Control of Spacecraft Using Two SGCMGS via LPV Control Theory," *Acta Astronautica*, Vol. 68, No. 7, 2011, pp. 1168–1175. doi:10.1016/j.actaastro.2010.10.001

[17] Tsiotras, P., and Doumtchenko, V., "Control of Spacecraft Subject to Actuator Failures: State-of-the-Art and Open Problems," *Journal of the Astronautical Sciences*, Vol. 48, No. 2, 2000, pp. 337–358.

[18] Yamada, K., Jikuya, I., and Kwak, O., "Rate Damping of a Spacecraft Using Two Single-Gimbal Control Moment Gyros," *Journal of Guidance, Control, and Dynamics*, Vol. 36, No. 6, 2013, pp. 1606–1623. doi:10.2514/1.60693

[19] Gui, H. C., Vukovich, G., and Xu, S. J., "Attitude Stabilization of a Spacecraft with Two Parallel Control Moment Gyroscopes," *Journal of Guidance, Control, and Dynamics*, Vol. 39, No. 3, 2016, pp. 728–735. doi:10.2514/1.G000982

[20] Gui, H. C., Jin, L., Xu, S. J., et al., "On the Attitude Stabilization of a Rigid Spacecraft Using Two Skew Control Moment Gyros," *Nonlinear Dynamics*, Vol. 79, No. 3, 2015, pp. 2079–2097. doi:10.1007/s11071-014-1796-0

[21] Yoon, H., and Tsiotras, P., "Spacecraft Adaptive Attitude and Power Tracking with Variable Speed Control Moment Gyroscopes," *Journal of Guidance, Control, and Dynamics*, Vol. 25, No. 6, 2002, pp. 1081–1090. doi:10.2514/2.4987

[22] Wie, B., Bailey, D., and Heiberg, C., "Rapid Multitarget Acquisition and Pointing Control of Agile Spacecraft," *Journal of Guidance, Control, and Dynamics*, Vol. 25, No. 1, 2002, pp. 96–104. doi:10.2514/2.4854

[23] Hughes, P. C., *Spacecraft Attitude Dynamics*, Dover Publ., New York, 2012, Chap. 3.

[24] Jin, L., and Xu, S. J., "Underactuated Spacecraft Angular Velocity Stabilization and Three-Axis Attitude Stabilization Using Two Single Gimbal Control Moment Gyros," *Acta Mechanica Sinica*, Vol. 26, No. 2, 2010, pp. 279–288. doi:10.1007/s10409-009-0272-4

[25] Horri, N. M., Palmer, P., and Hodgart, S., "Practical Implementation of Attitude-Control Algorithms for an Underactuated Satellite," *Journal of Guidance, Control, and Dynamics*, Vol. 35, No. 1, 2012, pp. 40–45. doi:10.2514/1.54075

[26] Chaurais, J. R., Ferreira, H. C., Ishihara, J., et al., "Attitude Control of an Underactuated Satellite Using Two Reaction Wheels," *Journal of Guidance, Control, and Dynamics*, Vol. 38, No. 10, 2015, pp. 2010–2018. doi:10.2514/1.G000145

[27] Zou, A. M., Kumar, K. D., and De Ruiter, A. H. J., "Spacecraft Attitude Control Using Two Control Torques," *Information Sciences*, Vol. 408, Oct. 2018, pp. 23–40. doi:10.1016/j.ins.2017.04.032

[28] Yu, S. H., Yu, X. H., Shirinzadeh, B., et al., "Continuous Finite-Time Control for Robotic Manipulators with Terminal Sliding Mode," *Automatica*, Vol. 41, No. 11, 2005, pp. 1957–1964. doi:10.1016/j.automatica.2005.07.001

[29] Lu, K. F., and Xia, Y. Q., "Adaptive Attitude Tracking Control for Rigid Spacecraft with Finite-Time Convergence," *Automatica*, Vol. 49, No. 12, 2013, pp. 3591–3599. doi:10.1016/j.automatica.2013.09.001

[30] Lappas, V. J., Steyn, W. H., and Underwood, C., "Design and Testing of a Control Moment Gyroscope Cluster for Small Satellites," *Journal of Spacecraft and Rockets*, Vol. 42, No. 4, 2005, pp. 729–739. doi:10.2514/1.7308

[31] Lappas, V., and Wie, B., "Robust Control Moment Gyroscope Steering Logic with Gimbal Angle Constraints," *Journal of Guidance, Control, and Dynamics*, Vol. 32, No. 5, 2009, pp. 1662–1666. doi:10.2514/1.43806